



LAWRENCE  
LIVERMORE  
NATIONAL  
LABORATORY

# TATB Thermal Decomposition: An Improved Kinetic Model for Explosive Safety Analysis

J. S. Moore, K. D. Morrison, A. K. Burnham, A. Racoveanu, J. G. Reynolds, B. Koroglu, K. R. Coffee, G. L. Klunder

August 31, 2023

Propellants, Explosives, Pyrotechnics

## **Disclaimer**

---

This document was prepared as an account of work sponsored by an agency of the United States government. Neither the United States government nor Lawrence Livermore National Security, LLC, nor any of their employees makes any warranty, expressed or implied, or assumes any legal liability or responsibility for the accuracy, completeness, or usefulness of any information, apparatus, product, or process disclosed, or represents that its use would not infringe privately owned rights. Reference herein to any specific commercial product, process, or service by trade name, trademark, manufacturer, or otherwise does not necessarily constitute or imply its endorsement, recommendation, or favoring by the United States government or Lawrence Livermore National Security, LLC. The views and opinions of authors expressed herein do not necessarily state or reflect those of the United States government or Lawrence Livermore National Security, LLC, and shall not be used for advertising or product endorsement purposes.

DOI: 10.1002/prop.202300237

# TATB Thermal Decomposition: An Improved Kinetic Model for Explosive Safety Analysis

Jason S. Moore<sup>\*[a]</sup>, Keith D. Morrison<sup>[a]</sup>, Alan K. Burnham<sup>[a]</sup>, Ana Racoveanu<sup>[a]</sup>, John G. Reynolds<sup>[a]</sup>, Batikan Koroglu<sup>[a]</sup>, Keith R. Coffee<sup>[a]</sup>, Greg L. Klunder<sup>[a]</sup>

**Abstract:** We investigate and model the cook-off behavior of 1,3,5-triamino-2,4,6-trinitrobenzene (TATB) to understand the response of explosive systems in abnormal thermal environments. Decomposition has been explored via conventional ODTX (one-dimensional time-to-explosion), PODTX (ODTX with pressure-measurement), PyGC-MS (pyrolysis gas chromatography mass spectrometry), TGA (thermo-gravimetric analysis), DSC (differential scanning calorimetry), and IR (infrared spectroscopy) experiments under isothermal and ramped temperature profiles. The data were used to fit rate parameters for proposed reaction schemes in a MATLAB thermo-chemical computational model. These parameterizations were carried out utilizing a genetic algorithm optimization method on LLNL's high-performance computing clusters, which enabled significant parallelization. These results include a multi-step reaction decomposition model, identification of likely autocatalytic gas-phase species, accurate high-temperature sensitization, and prediction of confined system pressurization. This model will be scalable to several applications involving TATB-based explosives, like LX-17, including thermal safety models of full-scale systems.

**Keywords:** TATB, Explosive Safety, Reaction Kinetics, Modeling, Thermal Response

## 1 Introduction

Understanding the thermal response of energetic material is critical for response prediction and safe handling during and after exposure to high temperatures in accident scenarios. Formulations of the high explosive (HE) 1,3,5-triamino-2,4,6-trinitrobenzene (TATB), such as LX-17 (92.5% TATB, 7.5% Kel-F) and PBX-9502 (95% TATB, 5% Kel-F), are currently employed in industrial and military applications, due to their high thermal stability and low shock sensitivity. However, many questions about the thermal decomposition pathways of TATB still remain unanswered in the literature, including conflicting conclusions as to the effect of confinement<sup>[1]</sup> and whether the dominant decomposition mechanism includes gas-phase species. Herein, we report on recent experimental and modeling advances that significantly further the understanding of the thermal breakdown of TATB.

Recent work by Hobbs and Kaneshige<sup>[1]</sup> included the effect of the initial water content, which is typically on the order of thousands of ppm, as determined by Small, Glascoe, and Overturf.<sup>[2]</sup> Including the water vapor-liquid equilibrium significantly improves the accuracy of pressure predictions during early decomposition, which is particularly important in low-

confinement systems. Furthermore, several studies have shown that the decomposition of TATB yields a large quantity of water; experimental<sup>[3],[4]</sup> and computational<sup>[5],[6]</sup> studies indicate that a likely first step in decomposition is an intramolecular condensation reaction to form the benzomonofurazan (F1), 5,7-dinitroisobenzofuran-4,6-diamine. TATB also reacts to form the benzomonofuroxan, 4,6-diamino-5,7-dinitrobenzo[c][1,2,5] oxadiazole 1-oxide, although in significantly smaller amounts. However, little has been reported about what happens between these initial reactions and final thermal runaway. Experiments have shown that these intermediates can continue to dehydrate, and the furoxan species can be significantly less stable.<sup>[4],[7]</sup> Additionally, some reported gas products, such as HCN, are highly hazardous and may require more precautions for first responders.<sup>[8]</sup>

Previous experiments related to hazards analysis have largely focused on thermal “cook-off” behavior in experiments such as the one-dimensional time to explosion (ODTX),<sup>[9]</sup> which can be augmented with pressure measurements (PODTX).<sup>[10]</sup> Here, the “one-dimensional” refers to the use of a sphere of explosive material, allowing spatial considerations to largely be reduced to only a function of radius. This setup, shown in Figure 1, has been described elsewhere. In brief, a half-inch diameter sphere of HE is either exposed to a step-change in temperature by delivery to preheated anvils, which are rapidly closed, or subjected to controlled temperature ramps, sometimes with isothermal holds. This system can also be used to thermally damage samples to examine chemical and behavior changes without continuing to thermal runaway to assess changes in several safety metrics.<sup>[11]</sup> Critically, some partially decomposed samples have shown lower temperatures of thermal runaway.

[a] Jason S. Moore\*, Keith D. Morrison, Alan K. Burnham, Ana Racoveanu, John G. Reynolds, Batikan Koroglu, Keith R. Coffee, Greg L. Klunder  
Lawrence Livermore National Laboratory  
7000 East Avenue, Livermore, CA 94551  
E-mail: moore242@llnl.gov

Supporting information for this article is available on the WWW under <http://www.pep.wiley-vch.de> or from the author.

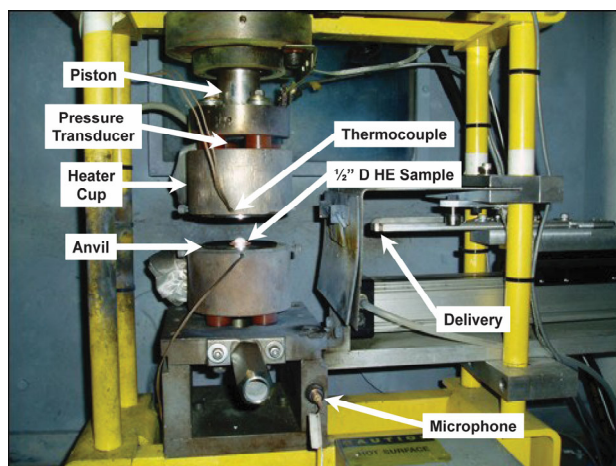


Figure 1. (P)ODTX experimental setup.

## 2 Modeling Details

As the earlier focus of experiments has largely been on end-point data, we previously proposed a reduced form of the reaction network,<sup>[12]</sup> excluding the furoxan species and later intermediates. However, recent PyGC-MS (pyrolysis gas chromatography mass spectrometry),<sup>[13]</sup> TGA (thermo-gravimetric analysis), and DSC (differential scanning calorimetry) experiments<sup>[14]</sup> have enabled a much more detailed analysis of thermal decomposition beyond those typically seen in (P)ODTX,<sup>[15]</sup> where only a few percent of the starting material is typically converted to products before thermal runaway, as illustrated in Figure 2.

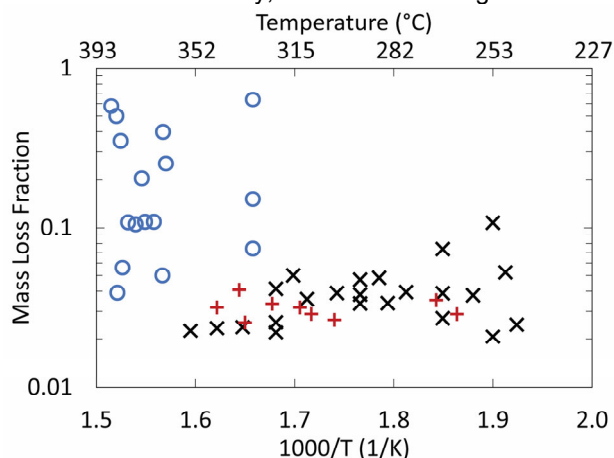


Figure 2. Comparison of final temperatures and mass loss fractions in ODTX (x), PODTX (+), and Simultaneous DSC/TGA (o) experiments.

The (P)ODTX experiments were modeled as a 0.5" diameter sphere of HE with radial symmetry surrounded by a 3" diameter shell of aluminum or stainless steel. For ODTX simulations, the aluminum shell was preheated to the appropriate temperature, allowing the adjacent surface of the HE to experience a rapid temperature change in the first fraction of a second of the calculation. For PODTX simulations, the temperature of the outer surface of a stainless-steel

shell was ramped at the corresponding experimental rate. Ramp rates were tested from 0.1 to 10 °C/min. While at lower ramp rates, the experiment is predicted to be mostly isothermal, at higher ramp rates, significant thermal gradients are expected to exist, including between the inner and outer surfaces of the anvil, necessitating modeling of the full thickness.

As TGA and DSC experiments were conducted on much smaller samples of 0.2 to 3 mg in a pinhole pan, a different simulation was used to model these experiments, consisting of small zone of HE material sitting on an aluminum block to simulate the temperature gradient in the aluminum sample pan. To account for the significant headspace, the gas-phase species are modeled as homogeneously mixed into a larger total volume denoted by  $V_r$ , the effective volume ratio of the gas to the solid, which experimentally is about 400 for the 40  $\mu$ L pans with 0.2 mg samples.

Our approach differs from previous modeling efforts in a few key respects. Firstly, our model uses only explicit chemical reactions, excluding any aspects lacking detailed mechanistic interpretation, such as Prout-Tompkins reactions.<sup>[16],[17]</sup> Additionally, solid explosives differ from many traditional kinetic systems due to the large effect of spatially varying factors. Thus, experiments were simulated using a method-of-lines<sup>[18]</sup> approach in MATLAB,<sup>[19]</sup> which simulated a discretized, one-dimensional geometry, including thermodynamics and chemical reactions with rates for each of the decomposition reactions,  $j$ , given by the Arrhenius equation

$$k_j = k_{0,j} \exp \left[ -\frac{E_{A,j}}{RT} \right] \quad (1)$$

where  $R$  is the ideal gas constant. The activation energy,  $E_A$ , and the natural log of the pre-exponential factor,  $k_0$ , were varied using a genetic algorithm<sup>[20]</sup> in MATLAB. The algorithm allows for separately calculating the objective function for every member of the population, enabling parallelization and flexibility in the use of computational resources.

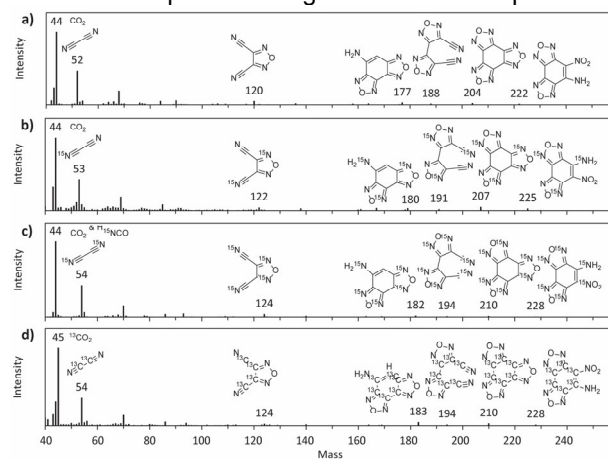
The objective function

$$\sum_{i=1}^{N_{exp}} \left( \ln \left( \frac{t_{sim,i}}{t_{exp,i}} \right) \right)^2 \quad (2)$$

was minimized, where  $t_{sim,i}$  and  $t_{exp,i}$  are the simulated and experimental times, respectively, for the  $i^{\text{th}}$  experiment for  $N_{exp}$  total experiments. Simulation stop times were determined using an "Event" function when the maximum temperature reached 1000 K, indicating thermal runaway, or the maximum pressure in the HE exceeded the holding pressure of 150 or 200 MPa, indicating a pressure burst. (See SI for full experimental data.) For TGA, the times at 5 and 50% mass loss were compared. For DSC, the width of the exothermic peak was compared at 10 and 50% maximum heat flow. Additionally, the temperature at the exotherm onset (defined here as 10% max heat flow) and maximum were compared.

### 3 Results and Discussion

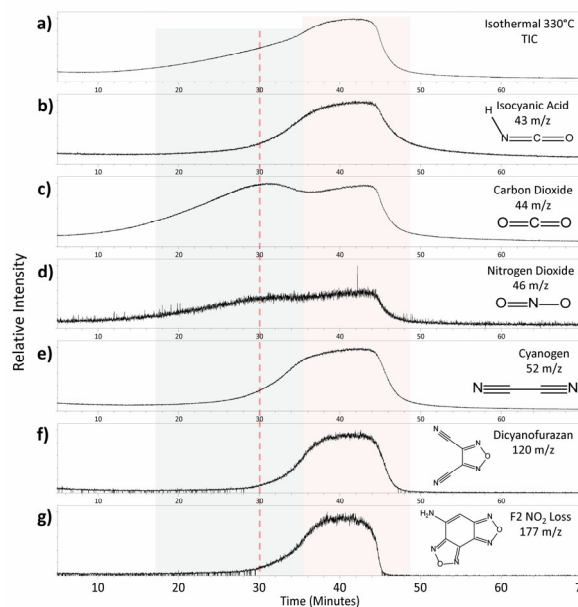
To further elucidate the species formed during thermal decomposition, TATB of high chemical purity, as well as  $^{13}\text{C}$ , D,  $^{15}\text{N}$ , and  $^{18}\text{O}$  isotopically-labeled TATB,<sup>[21],[22]</sup> were studied using PyGC-MS and Py-MS in EGA (evolved gas analysis) mode at elevated temperature (> 300 °C). These experiments are discussed in detail in Morrison, *et al.*<sup>[13]</sup> In brief, samples of masses from 100 to 330  $\mu\text{g}$  were studied in unconfined and foil-confined experiments under ramped and isothermal conditions, in which samples were loaded into a preheated oven. Figure 3 shows several of the primary masses measured at the highest total ion count near the end of thermal decomposition during 330 °C isothermal experiments with unlabeled,  $^{15}\text{N}$  amine-labeled,  $^{15}\text{N}$  amine- and nitro-labeled, and  $^{13}\text{C}$ -labeled TATB. Unfortunately, due to exchange with environmental water, the D and  $^{18}\text{O}$  labeled materials had much lower isotopic purities in the Py-MS experiments. However, the C and N labels are sufficient to identify many intermediate species during the TATB decomposition.



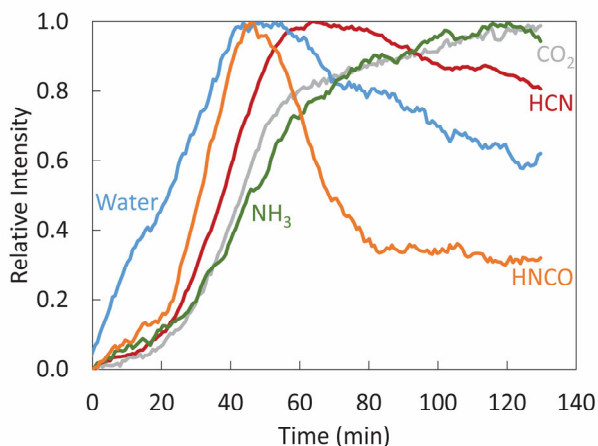
**Figure 3.** Mass spectra and selected chemical structures at peak ion count for a) unlabeled TATB, b)  $^{15}\text{N}$  amine-labeled TATB, c)  $^{15}\text{N}$  amine- and nitro-labeled TATB, and d)  $^{13}\text{C}$ -labeled TATB.

Figure 4 shows the total ion chromatogram (TIC) and the extracted ion chromatogram (EIC) for several selected species during a 10 °C/min ramped experiment. These analyses point to there being two phases in the decomposition of TATB. During the initial stage, large molecules are degraded to a range of solid intermediates. Up to three dehydrations occur, sequentially forming benzomonofurazan (F1), benzodifurazan (F2), and benzotrifurazan (F3) in what appears to be a low activation energy pathway that dominates at lower temperatures. Additionally, these molecules may also undergo a higher activation energy scission, more prevalent at higher temperatures,<sup>[5]</sup> resulting in  $\text{NO}_2$  loss from TATB, F1, and F2, as indicated by the F2 nitro loss species in Figure 4g. Some breakup of the TATB carbon backbone also occurs early, as indicated by the early formation of  $\text{CO}_2$ , which experiments with the  $^{13}\text{C}$  labeled TATB confirm is not exogenous but formed from the TATB itself.<sup>[23]</sup> The mass 188 species is F3 that has ring-opened at one of

the furazans and lost an oxygen, likely leading to a set of “unzipping” reactions.



**Figure 4.** Py-MS evolved gas analysis of isothermal (330 °C) confined TATB. a) Total ion count chromatogram. b-g) extracted ion chromatograms.



**Figure 5.** Concentration of major products measured in infrared spectra at 330 °C after 10 °C/min heating.<sup>[24]</sup>

However, as the Py-MS experiments used  $\text{N}_2$  as the carrier gas, compounds smaller than molecular weight 28 were not tracked. Incorporating the results from infrared spectroscopy (IR) experiments,<sup>[24],[25]</sup> shown in Figure 5, leads to the conclusion that the higher weight compounds are reactive intermediates that degrade further to small molecules:  $\text{H}_2\text{O}$ ,  $\text{HNCO}$ ,  $\text{HCN}$ ,  $\text{NH}_3$ , and  $\text{CO}_2$ . The time trend of the  $\text{HNCO}$ , which peaks early in the decomposition, suggests that it too is only an intermediate. The  $\text{HNCO}$  may react further with  $\text{H}_2\text{O}$ , which is not typically seen in sufficient quantity to fully account for all three dehydration reactions needed to form F3 from TATB, resulting in the  $\text{NH}_3$  and  $\text{CO}_2$ , which rise as  $\text{HNCO}$  falls. Additionally, the  $\text{HNCO}$  may interconvert between multiple isomers.<sup>[26], [27]</sup> Comparing the two figures shows that both experiments

yield similar peak decomposition times at around 40 minutes. However, as the IR cell is a sealed system, the tailing behavior is somewhat different.

Figure 4 shows that of the small molecules measured in the MS, only CO<sub>2</sub> and NO<sub>2</sub> are present in the first phase of decomposition. Thus, we conclude that NO<sub>2</sub> is likely to be autocatalytic in early decomposition, once enough of the initial reactions have proceeded to form it. Additionally, density functional theory (DFT) computations show that increasing crystal disorder lowers the barrier to further decomposition, possibly realigning a nitro group over a carbon in a neighboring ring. Water is also likely to aid hydrogen hopping during further dehydrations.<sup>[28]</sup> For the purposes of modeling, the early solid intermediates (SI) are taken to be in a range of species from mass 204 F3 to mass 120 3,4-dicyanofurazan (DCFA), itself an explosive.<sup>[29]</sup>

The second phase of the decomposition, wherein the majority of the TATB backbone is degraded, features prominent peaks of HNCO and C<sub>2</sub>N<sub>2</sub>. As shown in Figure 3, after dehydration, no hydrogen remains in any of the intermediate mass molecules. As these degrade, they release cyanide compounds, which we propose as the catalytic agent in the second decomposition phase. At the end of this second exotherm, approximately 30 wt% of the sample remains, which continues to pyrolyze slowly between 400 and 500 °C until approximately 21 wt% remains as an amorphous carbon nitride residue.<sup>[30], [31]</sup> This final 9% of mass loss is not included in the model.

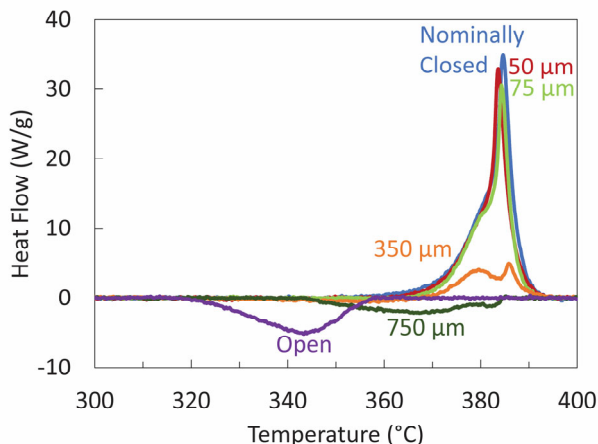
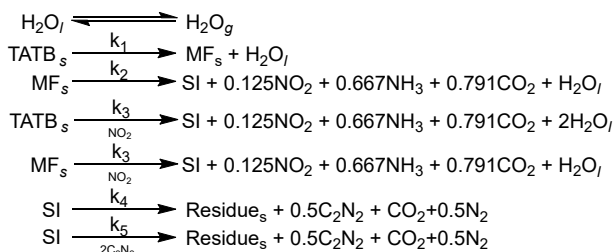
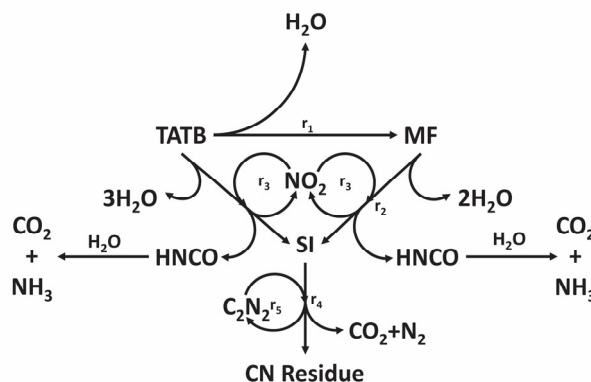


**Figure 6.** Effect of pin hole size on reaction heat flow at 10 °C/min.<sup>[32]</sup>

Our proposed reaction mechanism is shown in Scheme 1, where  $P$  is total pressure and the individual species are listed by the number of moles formed per mole of reaction. However, as with LLNL's hydrocode ALE3D,<sup>[33]</sup> the reaction rates are calculated based on species mass densities rather than molar concentrations. Kinetic parameters for each reaction are listed in Table 1 along with their 95% joint confidence interval, instead of error values for individual variables, as is often reported. The  $\Delta H_r$ , heat of reaction, for each step is calculated using the  $\Delta H_f$ , heat of formation, of each compound as given in literature (see

SI for full properties). The initial phase of TATB decomposition is often reported as endothermic. However, as shown in Figure 6, the endotherm is typically a result of sublimation. When sublimation is suppressed, as when using a small pinhole or a closed pan, no endotherm is seen.<sup>[32]</sup>



$$r_1 = k_{0,1}[\text{TATB}] \exp(-E_{A,1}/RT)$$

$$r_2 = k_{0,2}[\text{MF}] \exp(-E_{A,2}/RT)$$

$$r_3 = k_{0,3}P[\text{TATB}|\text{MF}][\text{NO}_2] \exp(-E_{A,3}/RT)$$

$$r_4 = k_{0,4}[\text{Solid Intermediates}] \exp(-E_{A,4}/RT)$$

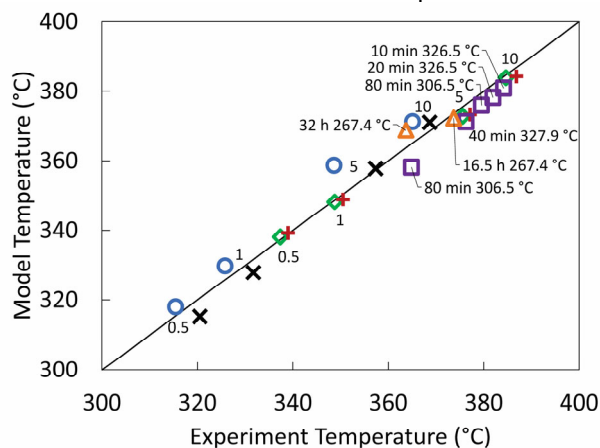
$$r_5 = k_{0,5}P^2[\text{Solid Intermediates}][\text{C}_2\text{N}_2]^2 \exp(-E_{A,5}/RT)$$

**Scheme 1.** TATB decomposition scheme. Solid intermediates represent a mix of species between DCFA and F3. Residue is primarily an amorphous carbon nitride.

**Table 1.** Parameters and 95% joint confidence intervals for reaction rates shown in Scheme 1.

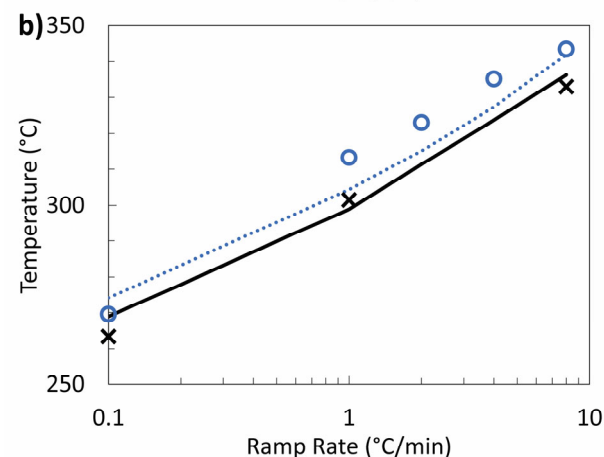
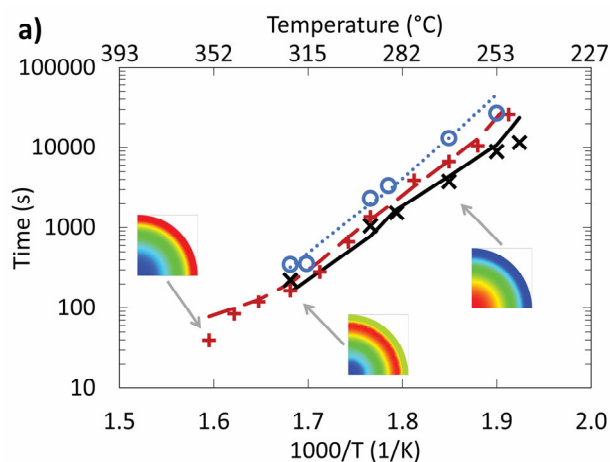
| Parameter     | Value | Units   | Error | $\Delta H_r$ (J/g) |
|---------------|-------|---|-------|--------------------|
| $\ln k_{0,1}$ | 7.1   | s <sup>-1</sup>                                     | 1.1   | 0                  |
| $E_{A,1}$     | 84.8  | kJ/mol  | 3.3   |                    |
| $\ln k_{0,2}$ | 49.8  | s <sup>-1</sup>                                     | 2.2   | -855.1             |
| $E_{A,2}$     | 277.1 | kJ/mol  | 5.9   |                    |
| $\ln k_{0,3}$ | 45.0  | cm <sup>3</sup> /g·s·MPa                            | 1.0   | -855.1             |
| $E_{A,3}$     | 225.1 | kJ/mol  | 5.7   |                    |
| $\ln k_{0,4}$ | 43.1  | s <sup>-1</sup>                                     | 1.7   | -1509.9            |
| $E_{A,4}$     | 254.6 | kJ/mol  | 37    |                    |
| $\ln k_{0,5}$ | 52.5  | cm <sup>6</sup> /g <sup>2</sup> ·s·MPa <sup>2</sup> | 1.0   | -1509.9            |
| $E_{A,5}$     | 244.0 | kJ/mol  | 6.0   |                    |

Figure 7 shows the effect of initial preheating on the TGA and DSC results. The model fits the results of both the shorter holds at higher temperatures and the thermal damage sensitization at lower temperatures in holds of several hours long, which previously reported mechanisms have not been able to capture.

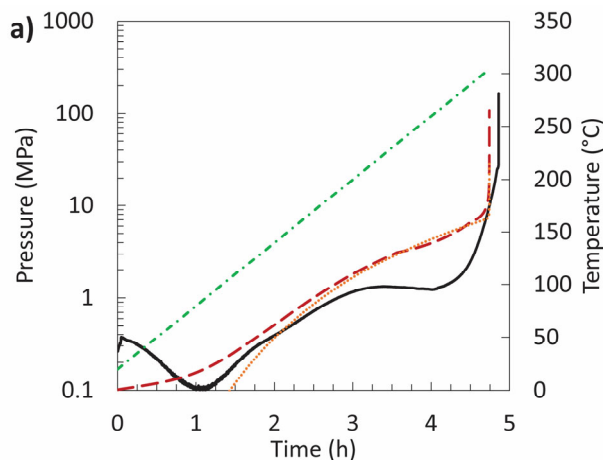


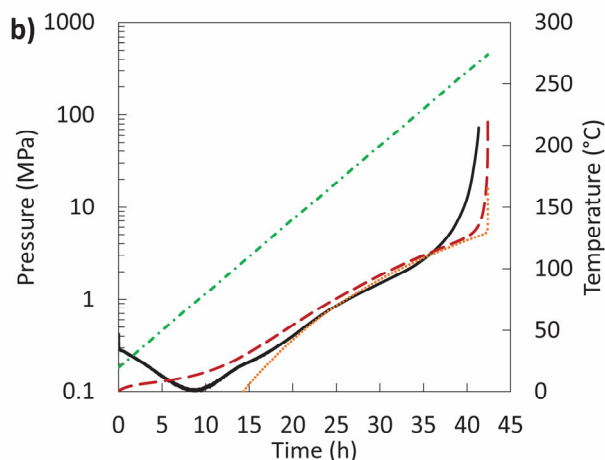
**Figure 7.** Effect of thermal damage on 5% TGA ( $\circ$ ), 50% TGA ( $\diamond$ ),  $T_{\text{onset}}$  ( $\times$ ), and  $T_{\text{max}}$  with no preheating ( $+$ ), short preheating ( $\square$ ), and long preheating ( $\triangle$ ). Points are labelled with heating rate or pretreatment conditions before 10 °C/min heating.<sup>[14]</sup>

Figure 8 compares results of modeled (P)ODTX LX-17 times to explosion at three different densities, displaying the effect of the gas pressure on the rate of autocatalysis. The insets show example temperature gradients within the HE at the end of the simulation, demonstrating the importance of radial effects of coupled chemistry and heat transfer. At the higher temperatures, the outer layer of HE reacts rapidly before heat can conduct into the center. At lower temperatures, heat fully conducts into the HE, and thermal runaway occurs at the center when reaction heat generation outpaces conduction. At lower temperatures still, thermal runaway may not occur since the reaction may not reach this threshold. Pressure results, which were not used to fit the model parameters, are given in Figure 9 for 86% TMD LX-17 at 1 and 0.1 °C/min, showing good agreement, as well as illustrating the importance of the water-steam equilibrium on the pressure during a large portion of the experiments before thermal runaway is approached.



**Figure 8.** Experiment (symbols) and model (lines) explosion/burst time for a) LX-17 ODTX: 98-100% TMD ( $\times$ ; solid), 94-97% TMD ( $+$ ; long dashed), and 85-89% TMD ( $\circ$ ; dotted); b) LX-17 PODTX results: 98% TMD ( $\times$ ; solid) and 86% TMD ( $\circ$ ; dotted).





**Figure 9.** LX-17 PODTX pressure with 86% TMD spheres at a) 1 °C/min ramp and b) 0.1 °C/min ramp. Experiment (black line), model (red dashed), steam equilibrium (orange dotted), and temperature (green dash-dot).

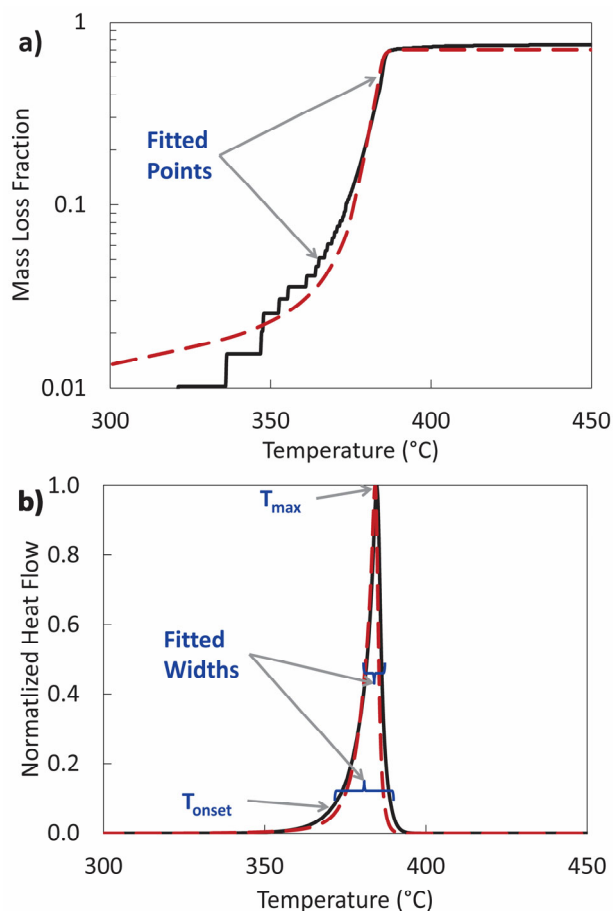


**Figure 10.** Results for 10 °C/min TATB a) TGA experiment (black solid line) and model (red dashed line); b) DSC experiment (black solid line) and model (red dashed line).

Comparison of the 10 °C/min TGA and DSC measurements<sup>[14]</sup> and simulations are shown in Figure 10, where the points used for data fitting are indicated. The early evaporation of the initial 0.15 wt% water is

evident in the mass loss curve. However, due to noise in the baseline of the experimental measurement, the initial portion is not shown. The model also captures the double peak nature of the measured heat flow. A similar comparison for the 10 °C/min to 330 °C isothermal experiments, as well as the calculated concentrations, is given in Figure 11, which further illustrates the two-stage nature of TATB decomposition.

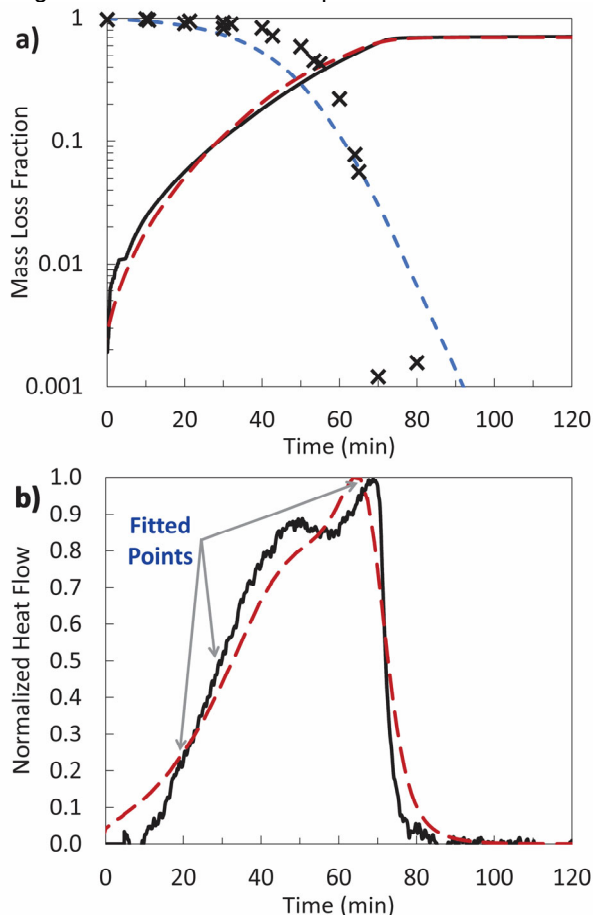


**Figure 11.** TATB 330 °C isotherm results after 10 °C/min ramp. a) TGA experiment (black solid line), model (red dashed line), and TATB experimental (x) and model (blue dashed line) concentration profiles; b) DSC experiment (black solid line) and model (red dashed line).

## 4 Conclusions

Data from a variety of experiments, including conventional ODTX, PODTX, Py-MS, TGA, DSC, and IR experiments under isothermal and ramped temperature profiles were combined to develop and fit rate parameters for a proposed TATB decomposition model in MATLAB. The multi-step reaction decomposition model accurately matches data from across these experiments, including identification of likely autocatalytic gas-phase species and prediction of confined system pressurization.

## Acknowledgements

This work was performed under the auspices of the U.S. DOE by Lawrence Livermore National Laboratory under contract DE-AC52-07NA27344. LLNS, LLC. The authors wish to thank Steve Strout, Evan Kahl, Taylor Miller, and Joseph Van Horn.

## References

- [1] M. L. Hobbs, M. J. Kaneshige, *The Journal of Chemical Physics* **2014**, *140*, 124203.
- [2] W. Small IV, E. A. Glascoe, G. E. Overturf, *Thermochimica Acta* **2012**, *545*, 90-95.
- [3] T. A. Land, W. J. Siekhaus, M. F. Foltz, in *10th International Detonation Symposium*, Boston, **1993**, pp. 181-189.
- [4] J. Sharma, J. W. Forbes, C. S. Coffey, T. P. Liddiard, *Journal of Physical Chemistry* **1987**, *91*, 5139-5144.
- [5] C. J. Wu, L. E. Fried, *Journal of Physical Chemistry A* **2000**, *104*, 6447-6452.
- [6] Q. Wu, H. Chen, G. Xiong, W. Zhu, H. Xiao, *Journal of Physical Chemistry C* **2015**, *119*, 16500-16506.
- [7] R. R. McGuire, Lawrence Livermore National Laboratory, UCRL-52353, **1978**.
- [8] E. Catalano, C. E. Rolon, *Thermochimica Acta* **1983**, *61*, 37-51.
- [9] P. C. Hsu, G. Hust, W. M. Howard, J. L. Maienschein, in *14th International Detonation Symposium*, LLNL-CONF-425264, Coeur d'Alene, ID, **2010**, pp. 984-990.
- [10] P. C. Hsu, S. A. Strout, J. G. Reynolds, E. M. Kahl, A. Hye, J. S. Moore, M. A. McClelland, M. Gresshoff, G. F. Ellsworth, T. E. Healy, in *16th International Detonation Symposium*, LLNL-CONF-754146, Cambridge, MD, **2018**, pp. 345-353.
- [11] E. M. Kahl, P. C. Hsu, K. R. Coffee, B. J. Yancey, A. J. Nelson, H. E. Mason, G. F. Ellsworth, T. E. Healy, J. C. Crowhurst, T. W. Myers, J. G. Reynolds, in *16th International Detonation Symposium*, Cambridge, MD, **2018**, pp. 1642-1652.
- [12] J. S. Moore, M. A. McClelland, P. C. Hsu, G. F. Ellsworth, E. M. Kahl, H. K. Springer, in *16th International Detonation Symposium*, Cambridge, MD, **2018**, pp. 936-945.
- [13] K. Morrison, K. R. Coffee, J. S. Moore, B. Koroglu, A. K. Burnham, J. G. Reynolds, *Propellants, Explosives, Pyrotechnics* **2023**, DOI: prep.202300268.
- [14] A. K. Burnham, K. R. Coffee, G. L. Klunder, A. F. Panasci-Nott, J. G. Reynolds, *Propellants, Explosives, Pyrotechnics* **2023**, DOI: prep.202300121.
- [15] When ODTX and PODTX are discussed together, "(P)ODTX" is used.
- [16] E. G. Prout, F. C. Tompkins, *Transactions of the Faraday Society* **1944**, *40*, 488-498.
- [17] J. Koerner, J. Maienschein, A. Burnham, A. Wemhoff, in *North American Thermal Analysis Society 35th Annual Conference*, East Lansing, MI, **2007**.
- [18] S. C. Chapra, R. P. Canale, *Numerical Methods of Engineers*, McGraw-Hill, New York, **2002**.
- [19] MATLAB, The MathWorks, Inc., Natick, MA, **2022**.
- [20] R. Storn, K. Price, *Journal of Global Optimization* **1997**, *11*, 341-359.
- [21] A. Racoveanu, K. R. Coffee, A. F. Panasci-Nott, B. Koroglu, C. A. Colla, J. R. I. Lee, K. D. Morrison, J. G. Reynolds, *Propellants, Explosives, and Pyrotechnics* **2023**, DOI: prep.202300185.
- [22] J. G. Reynolds, A. Racoveanu, A. K. Burnham, J. S. Moore, K. R. Coffee, A. F. Panasci-Nott, K. D. Morrison, G. L. Klunder, J. D. Van Horn, in *23rd Biennial Conference of the APS Topical Group on Shock Compression of Condensed Matter* Lawrence Livermore National Laboratory, Chicago, **2023**.
- [23] K. D. Morrison, A. Racoveanu, J. S. Moore, A. K. Burnham, B. Koroglu, K. R. Coffee, A. F. Panasci-Nott, G. L. Klunder, B. A. Steele, M. A. McClelland, J. G. Reynolds, *Nature Scientific Reports* **2023**, 21256.
- [24] B. Koroglu, J. C. Crowhurst, E. M. Kahl, J. S. Moore, A. Racoveanu, H. E. Mason, D. G. Weisz, J. G. Reynolds, A. K. Burnham, *Propellants, Explosives, Pyrotechnics* **2021**, *46*, 1352-1366.
- [25] G. L. Klunder, N. K. Muetterties, E. M. Kahl, P. E. Spackman, P. C. Hsu, in *16th International Detonation Symposium*, Cambridge, MD, **2018**, pp. 122-127.
- [26] M. S. Lowenthal, R. K. Khanna, M. H. Moore, *Spectrochimica Acta Part A* **2002**, *58*, 73-78.
- [27] S. Nourry, E.-L. Zins, L. Krimab, *Physical Chemistry Chemical Physics* **2015**, *17*, 2804-2813.
- [28] B. A. Steele, *Journal of Applied Physics* **2023**, *133*, 075902.
- [29] E. C. Johnson, E. J. Bukowski, R. C. Sausa, J. J. Sabatini, *Organic Process Research and Development* **2019**, *23*, 1275-1279.
- [30] J. G. Reynolds, N. K. Muetterties, A. J. Nelson, H. E. Mason, J. S. Moore, K. R. Coffee, E. M. Kahl, *Propellants, Explosives, Pyrotechnics* **2021**, *46*, 1136-1149.
- [31] E. M. Kahl, N. K. Muetterties, A. J. Nelson, H. E. Mason, J. V. Crowhurst, K. R. Coffee, J. S. Moore, J. G. Reynolds, in *American Physical Society: Shock Compression of Condensed Matter*, Portland, OR, **2020**.
- [32] B. Koroglu, A. K. Burnham, I. Mashiana, A. Racoveanu, C. Arose, J. C. Crowhurst, J. G. Reynolds, *Propellants, Explosives, Pyrotechnics* **2023**, *48*, e202300124.
- [33] C. Noble, A. Anderson, N. Barton, J. Bramwell, A. Capps, M. Chang, J. Chou, D. Dawson, E. Diana, T. Dunn, D. Faux, A. Fisher, P. Greene,

I. Heinz, Y. Kanarska, S. Khairallah, B. Liu, J. Margraf, A. Nichols III, R. Nourgaliev, M. Puso, J. Reus, P. Robinson, A. Shestakov, J. Solberg, D. Teller, P. Tsuji, C. White, J. White, LLNL-TR-732040, Lawrence Livermore National Laboratory, **2017**.

Received: ((will be filled in by the editorial staff))

Revised: ((will be filled in by the editorial staff))

---

## Graphical Abstract

